Title: Partitioning multi-source uncertainties in simulating nitrogen loading in stream water using a coherent, stochastic framework: Application to a rice agricultural watershed in subtropical China

Authors: Qiumei Ma[1], Lihua Xiong[1]*, Yong Li[2], Siyue Li[3], Chong-Yu Xu[1, 4]

[1] State Key Laboratory of Water Resources and Hydropower Engineering Science, Wuhan University, Wuhan 430072, China

[2] Changsha Research Station for Agricultural & Environmental Monitoring and Key Laboratory of Agro-ecological Processes in Subtropical Regions, Institute of Subtropical Agriculture, Chinese Academy of Sciences, Hunan, 410125, China

[3] Chongqing Institute of Green and Intelligent Technology, Chinese Academy of Sciences, Chongqing 400714, China

[4] Department of Geosciences, University of Oslo, P.O. Box 1022 Blindern, N-0315 Oslo, Norway

Corresponding author: Lihua Xiong, tel. +86 13871078660, fax +86 27 68773568, e-mail: xionglh@whu.edu.cn

Type of Paper: Primary Research Article

Abstract

Uncertainty is recognized as a critical consideration for accurately predicting stream water nitrogen (N) loading, but identifying the relative contribution of individual uncertainty sources within the total uncertainty remains unclear. In this study, a powerful method, referred to as the Bayesian inference combined with analysis of variance (BayeANOVA) was adopted to detect the timing and magnitude of multiple uncertainty sources and their relative contributions to total uncertainty in simulating daily loadings of three stream water N species (ammonium-N: NH_4^+-N, nitrate-N: NO_3^--N and total N: TN) in a rice agricultural watershed (the Tuojia watershed) as influenced by non-point source N pollution. Five sources of uncertainty have been analyzed in this study, which arise from model structure, parameters, inputs, interaction effects between parameters and inputs, and internal variability (induced by random errors of model or environment). The results show that uncertainty in parameters relating to the processes of both N and hydrologic cycles contributed the largest fractions of total uncertainty in N loading simulations (58.83%, 63.48% and 61.64% for NH_4^+-N, NO_3^--N and TN loading, respectively). Additionally, three of the largest uncertainties (i.e. parameters, inputs and interaction effects) in all three simulated N loadings were on average significantly greater in the rice-growing season relative to the fallow season, primarily due to the excess fertilization application during the rice-growing season. The predicted TN uncertainty was mainly attributed to the inaccuracy of NO_3^--N simulation, which contributed to 75.48% of predicted TN uncertainty. It is concluded that reducing the parameter uncertainty of NO_3^--N loading simulation during the rice-growing season is the key factor to improving stream water N modeling precision in rice agricultural watersheds.

Keywords: Stream water nitrogen loading; Multi-source uncertainties; Bayesian;

Rice agricultural watershed

1. Introduction

Hydrologic nutrient transport models are practical tools to investigate watershed nutrient (such as nitrogen and phosphorus) dynamics, which have important implications in biogeochemical cycles (Bosch, 2008; Jiang et al., 2015; Qian et al., 2017). Excessive riverine nitrogen (N) content, responsible for N eutrophication and non-point source pollution of aquatic resources, has raised increasing concern worldwide (Bouraoui and Grizzetti, 2014; Eshleman et al., 2013; Hamilton, 2012; Wang et al., 2016). With growing interest in predicting the impact of climate change and human activity on watershed N, hydrologic N models are widely applied by environment managers and decision makers (Alexander et al., 2002; Bardule et al., 2017; Chen et al., 2014).

However, considerable uncertainty inherent in the predictions of N processes is a major obstacle to model applications for effectively managing stream water N (Jiang et al., 2015). Overvaluation of hydrologic N model uncertainty will lower utility values of the model, while undervaluation of uncertainty may lead to the inability to accurately capture the dominant observational trends. Therefore, analyzing uncertainty that originates from potential sources is one of the most important aspects of hydrologic N modeling (Hrachowitz et al., 2013; Wellen et al., 2015).

Multiple sources of uncertainty affect the accuracy of hydrologic N models (Arabi et al., 2007; Arhonditsis et al., 2008). The first uncertainty source is related to model structure. A key issue of N modeling is the multiple biogeochemical processes among various N species in watershed discharge, and our process-based models cannot capture the detailed reactions. Typically, nitrification and denitrification processes occur at the same time and are mutually affected by each other. In this sense,

poor model performance indicates a knowledge gap of dominant processes depicting N cycling, causing conceptual bias and structural misrepresentations (i.e. structure uncertainty) (Arhonditsis et al., 2008). The second source of predictive uncertainty originates from over parameterization and equifinality (i.e. parameter uncertainty) in complex N models (Beven, 1993, 2006). Ideally, a model should have a parsimonious set of parameters, along with a high degree of mechanistic detail to depict the dominant controlling processes in the fate of N (Young and Parkinson, 2002). The third aspect of uncertainty is linked to forcing inputs. Input data, such as precipitation, soil, temperature and land use/cover, play a significant role in driving watershed N simulations (Du et al., 2017; Harmel and Smith, 2007), whereas the amount of information contained in input data is often limited. This is partly due to the absence of near-continuous monitoring, leading to input uncertainty. Two kinds of statistical components, i.e., the interaction effects between two of the three uncertainties listed above (Lovenduski et al., 2016) and some random variability from the model itself or the internal environment in nature (namely internal variability) (Ahn et al., 2016), can have more than negligible contributions on the total uncertainty in model applications. Apart from the sources of uncertainty discussed above, there are other aspects, beyond anthropogenic episteme, which potentially influence N prediction.

In practice, the most commonly used approaches for analyzing uncertainty sources of stream N dynamic modeling include two categories: single-source and multi-source uncertainty analysis. For single-source uncertainty analysis, the parameter uncertainty in N process simulation has been widely investigated in different regions and watersheds (Alexander et al., 2002; Arabi et al., 2007). As for multi-source uncertainty analysis, some studies have documented the parameter uncertainty combined with output/prediction uncertainty (Gardner et al., 2011; Jiang

et al., 2015), observation data uncertainty (Du et al., 2017) and structure errors (Harmel et al., 2006; McIntyre and Wheater, 2004), to name a few. Additionally, a conceptual framework entitled the integrated uncertainty of multiple sources was proposed by Sullivan et al. (2004) for N deposition simulation in regional stream systems, and Yen et al. (2014) used this framework in watershed modeling. The drawback of these pioneering methods is that current sources of uncertainty are neither entirely incorporated nor considered under an integrated statistical framework. Thus far, explicit partition and comprehensive comparison of multiple sources of uncertainty in stream water N modeling have not yet been examined.

To solve this problem of partitioning multiple uncertainty sources, a powerful statistical approach, referred to as the Bayesian inference combing analysis of variance (BayeANOVA), was developed (Northrop and Chandler, 2014). The analysis of variance (ANOVA) method focuses on seeking a full interpretation of various sources of the total uncertainty (Lovenduski et al., 2016; Yip et al., 2011), while the Bayesian method introduces random effects into the partitioned multi-source uncertainty components generated from a finite population, and thus, it circumvents the problem of a sparse and highly unbalanced dataset. Traditionally, the BayeANOVA approach has been considered to characterize the multi-source uncertainties in climate or hydrologic variables regarding global climate models (Hawkins and Sutton, 2009; Hawkins and Sutton, 2011; Kudo et al., 2017; Lovenduski et al., 2016; Yip et al., 2011) but without the inclusion of stream water nutrient constituents. We adopted this model-based BayeANOVA approach for partitioning and quantifying the multiple sources of stream water N modeling uncertainty.

Hence, the main objective of this paper was to establish and apply the

BayeANOVA approach for explicitly partitioning individual uncertainty sources and comparing their relative contributions to the total uncertainty in simulating daily stream N loading. To apply the proposed method, we selected three N species (ammonium-N: NH_4^+-N, nitrate-N: NO_3^--N and total N: TN) in a rice agricultural watershed, the Tuojia watershed in subtropical region of China. These three N species are critical constituents that reflect environmental risk in the streams. However, the uncertainty sources in modeling these three N species have not yet been investigated.

The remainder of the paper is organized as follows: In Section 2, the Tuojia watershed and available datasets are described. In Section 3, the framework, coupling the ensemble output of Catchment Nutrient Management Model (CNMM) with the partitioning procedure of BayeANOVA, is developed. Then in Section 4, the timing and magnitude of multi-source uncertainties in simulating N loadings and relative contributions to the total uncertainty are examined. Section 5 discusses the results, and finally, Section 6 concludes the study.

2. Study area and data acquisition

The Tuojia watershed, located at Jinjing Town (112°56′-113°36′E; 27°55′-28°40′N; elevation: 43-460 m) of Hunan Province, China, topographically represents floodplains and hilly landscape, covering an area of 52.1 km^2 (Fig. 1a). The land use mainly consists of Masson pine (*Pinus massoniana Lamb*) woodlands (58.0%) and rice paddy fields (32.2%). Paddy fields are the dominant agricultural land use type, primarily located in valleys and floodplains along with streams. Rice is cropped twice a year, with the early rice growing during mid-April to the end of June and late rice growing during mid-July to the mid-October. There is no crop growing in the paddy fields during the fallow season from mid-October to the following mid-April. The study area belongs to a typical subtropical monsoon climate, and receives 1,400 mm

yearly rainfall on average, of which more than 68.4% occurs during the months of April-August. The mean annual air temperature is 17.5℃. The main stream begins from the northern forest areas and flows through paddy fields and ditches before discharging to the southeast outlet (Fig. 1b).

The Tuojia watershed was selected as the study area for the following reasons: Previous studies conducted worldwide (Bouman et al., 2007; Krupa et al., 2011), report that severe N pollution is linked to agricultural watershed featured by rice cropping. Rice agriculture characterizes unique crop rotation, fertilization and land management and, therefore, has indirect connections with N chemical composition, concentration and loading in watershed streams. China has the second-largest area of rice agriculture, resulting in widespread N pollution. Therefore, investigating stream water N has significant importance to agricultural production and socio-economic development in these areas.

<Fig. 1>

Multiple databases were used in this study, including variables of meteorology, hydrology and water chemistry in the Tuojia watershed, which have been monitored by the Institute of Subtropical Agriculture, Chinese Academy of Sciences since 2010. Instantaneous discharge data were automatically collected every 15 minutes, and thereafter, the daily cumulative streamflow was calculated. A stream water sampling campaign, with the average interval of 10 days from November 2010 to October 2013, was conducted at approximately 0.2 m below the water surface at the outlet of the Tuojia watershed. Briefly, each water sample was divided into two portions: the first portion was dissolved in a $K_2S_2O_8$–NaOH solution to determine the TN concentration using a continuous flow analyzer method; the other was filtered through a 0.45-μm membrane, and the NH_4^+-N and NO_3^--N concentrations were determined in the filtrate,

based on the modified Berthelot reaction and cadmium reduction method, respectively, using a continuous flow analyzer (Tecator FIA Star 5000 analyzer, Foss Tecator, Sweden). Daily N loading from the watershed was calculated by multiplying the stream N concentration and corresponding daily amount of stream discharge, then dividing the covering area of the watershed (Eq. (1)).

$$L_N = \frac{\sum_{i=1}^{n} Q \times C}{10^3 Ar} \quad (1)$$

where L_N denotes the estimated daily N loading (kg km^{-2} d^{-1}), Q is the instantaneous discharge (m^3 s^{-1}), C is the concentration of NH_4^+-N, NO_3^--N or TN (mg L^{-1}), i is the *ith* second in one day (i = 1,2,3… n), and Ar is the area of watershed (km^2).

Meteorological data, including daily precipitation, wind speed, short/long wave radiation, air temperature and relative humidity were recorded by three meteorological stations in the Tuojia watershed during the same time period as the hydrologic-water quality data. All data, exhibited in Fig. 2, were tested for their representativeness and reliability. For the meteorological data, the representativeness was commonly quantified by the regional coefficient of variation (c.v.) at each time step (Bhowmik and Costa, 2015; Hill et al., 2006). Accordingly, the set of meteorological data from three meteorological stations (see Fig. 1b) in this study area was used to calculate the average c.v. value. All meteorological indices were considered highly representative. The reliability of all datasets used was realized by statistical pre-processing before modeling, i.e., interpolating missing observed values and diagnosing outliers. Specifically, the autoregressive moving averaging approach (ARMA(2, 1), Eq. (2)) was used to interpolate missing data (Valipour et al., 2013).

$$Y_t = a_1 Y_{t-1} + a_2 Y_{t-2} + \varepsilon_t + b_1 \varepsilon_{t-1} \quad (2)$$

where ε_t and ε_{t-1} comply with white noise distribution with zero mean and

constant variance; and Y_t is the missing data at time step t. In the datasets used, the percentage of missing data was very small (< 5% of total data length).

A method coupling the maximum-value test with experience-based judgment was used to remove the outliers or outlying observations (Chebana et al., 2012).

<Fig. 2>

3. Methods

The proposed framework for partitioning and quantifying each uncertainty source is presented in Fig. 3. The background of the selected hydrologic nutrient model (CNMM) is first briefly described in Section 3.1. Schemes across different model structures, parameter sets and input data, were then configured for CNMM to generate ensemble model outputs in Section 3.2. Finally, the BayeANOVA approach, which couples ANOVA with Bayesian inference, is outlined in Section 3.3.

The total uncertainty in predicting the loadings of three N species (ammonium-N: NH_4^+-N, nitrate-N: NO_3^--N and total N: TN) was partitioned into five sources: model structure, parameters, forcing inputs, interaction effects between parameters and inputs, and internal variability (induced by random errors of model or environment). It is important to note that we only considered the interaction effects between parameter and input uncertainty. This is because previous studies indicate the suitability of a specific parameter set to the model system depends on the given input scenario and vice versa (Shields and Tague, 2012). For the relatively small structure uncertainty and the purpose of controlling complexity, we neglected the interaction effects between structure and other source uncertainties. Consequently, it was hypothesized that the five different sources of uncertainty are statistically independent, except for the interaction effects existing between parameter and input uncertainty.

3.1 Background of Catchment Nutrient Management Model (CNMM)

As a physically-based and spatially-distributed hydrologic nutrient model, CNMM can simulate multiple processes, including water dynamics, plant-soil carbon-nitrogen-phosphorus cycling, and stream nutrient transfer and loss via runoff (Li et al., 2007). The calculation of CNMM is driven by meteorological observations, and its discretization in space is supported by the ArcGis platform, which can extract the information of Digital Elevation Model (DEM) and land use types. Multi-scale spatial-time steps are available for CNMM to simulate key biogeochemical processes. One day and 100 m were chosen as the temporal and spatial steps for the discretization scheme in this study. Considering N modeling using CNMM, the advantage lies in the integration of the hydro-ecological process, which couples a hydrologic-water quality module and a crop growth module to influence watershed N processes. One module facilitates the design of hydrologic-N process in stream and solute N transport in soil water, while the other module considers the absorption of water, nutrients and light by vegetation. CNMM is widely used for agricultural management practice and environmental risk assessment in subtropical agricultural watersheds of China. The detailed description of CNMM can be found in a recently published work by Li et al. (2017).

3.2 Configuration of individual model solution in CNMM

Schemes across different model structures, parameter sets and forcing inputs of the CNMM model are outlined as follows: As for the model structure uncertainty, unlike multi-model inter-comparison experiments used in previous studies (Duan et al., 2006; Lindenschmidt et al., 2007), we introduced three versions of CNMM (i.e. the basic CNMM added two modified versions) to test structure uncertainty. On the basis of CNMM, two functions controlling N cycle processes in soil and stream were changed

to generate modified versions. The first modification was to remove the function of N uptake by plants, affecting the storage of soil N and indirectly changing stream water N content. The second was to change a rate coefficient descripted by the Streeter-Phelps formula (Eq. (3)) used in diffusion-convection equation of in-stream N transformation. The modification made the rate coefficient a specified constant instead of a water temperature-dependent variable. The temperature-dependent coefficient, X_T can be written as:

$$X_T = X_{20}\theta^{(T-20)} \tag{3}$$

where X_{20} is the coefficient at the standard temperature (20℃); θ is an empirical value; and T is the observed temperature.

To quantify parameter uncertainty and its interactive effects on precipitation input, ten sensitive parameters, including four hydrologic parameters (three soil moisture related parameters and one stream channel parameter) and six N-process parameters (Table 1), were selected through literature investigation (Liang et al., 2016; Uniyal et al., 2015). Furthermore, the specific parameter set was classified into three levels for analyzing uncertainty linked to parameters, based on the optimal defaults and prior range recommended by Brown and Barnwell (1987) (Table 2).

<Table 1>

Precipitation, which drives multiple hydrologic and biogeochemical processes (Gao et al., 2014), was selected as the configuration variable of the forcing input. To concisely consider the input uncertainty of CNMM, a fixed sample from uniform distribution, instead of random sample from normal distribution, was used to estimate the variability of precipitation. The precipitation input was set to seven hypothetical levels, ranging in ±50% of raw measurements at each time step, *t* (Table 2).

In particular, to analyze the internal variability arising from random model errors

or natural internal processes in the environmental system (e.g. variability in climate), each individual CNMM solution was performed a number of times ranging from 1 to 4 (see the subscript *m* in Section 3.3). Each CNMM routine was primed with a "warm-up" period of ten months (January to October 2010) to allow the model to reach a steady state. Additionally, in the post-processing of the CNMM output, all simulated streamflow and N loadings were statistically downscaled using a polynomial fit model over the study period. Then, they were separated based on the rice-growing/fallow season to further compare the contrasting effect of all uncertainty sources.

<Table 2>

3.3 Construction of statistical framework for partitioning total uncertainty

After the individual model solution was defined, a three-step statistical method, the BayeANOVA approach, used to partition total uncertainty was derived. The BayeANOVA approach characterizes integration of variance decomposition and Bayesian random sampling, addressing the problem of data unbalance and sparseness in multi-dimensional space. First, the variances of individual model solutions, representing 5-source uncertainties of streamflow and three N loadings, were calculated using classical ANOVA based on respective finite-populations. Then, the standard deviations of individual model solutions, corresponding to the 5-source uncertainties, were estimated using the Bayesian stochastic method coupled with a half-Cauchy prior distribution. Finally, Bayesian inference was employed to obtain the 95% confidence intervals of simulated streamflow and N loadings, based on the ensemble output derived from ANOVA.

The total uncertainty in simulating streamflow or N loadings can be quantified on the basis of variance (U^2) (Eq. (4)) or standard deviation (U) (Eq. (5)) of all the

predictions in a given time. The total variance U^2 is equal to the sum of the variances due to model structure U_S^2, parameter set U_P^2, model input U_I^2, interaction effects between parameters and inputs U_{PI}^2, and system internal variability U_v^2:

$$U^2 = U_S^2 + U_P^2 + U_I^2 + U_{PI}^2 + U_v^2 \tag{4}$$

where U^2 on the left side of Eq. (4) is the variance across all configuration combinations.

$$U = \sqrt{\frac{\sum_{i=1}^{N_S}\sum_{j=1}^{N_P}\sum_{k=1}^{N_I}\sum_{m=1}^{N_v}(Y_{ijkm} - Y_{....})^2}{N_S \times N_P \times N_I \times N_v}} \tag{5}$$

where N_S, N_P, N_I and N_v are the number of structure versions, parameter sets, input levels and internal variability, respectively, and in our case study, N_S = 3, N_P = 6, N_I = 7, and $N_v \le 4$; Y_{ijkm} represents the specified output (streamflow or N loadings) of an individual model run; and $Y_{....}$ is the mean of all Y_{ijkm}, which can be derived as:

$$Y_{ijkm} = f_{str}(\mathrm{S}, \mathrm{I}, \theta) \quad \text{or} \quad Y_{ijkm} = f_{L_N}(\mathrm{S}, \mathrm{I}, \theta) \tag{6}$$

where $f_{str}()$ and $f_{L_N}()$ are the ensemble functions in CNMM for modeling stream discharge and stream water N loadings, respectively; *S*, *I*, and θ denote the structure, input, and parameter set, respectively, within a specific model solution.

In the ANOVA model, the form of Y_{ijkm} can be defined as:

$$Y_{ijkm} = \mu + \alpha_i + \beta_j + \gamma_k + \delta_{jk} + \varepsilon_{ijkm},\ i = 1,...,\mathrm{N}_S,\ j = 1,...,\mathrm{N}_P, k = 1,...,\mathrm{N}_I,\ m = 1,...,\mathrm{N}_v \tag{7}$$

where μ (equal to $Y_{....}$) is the mean discharge or N loadings; the parameters α_i, β_j, γ_k, δ_{jk} and ε_{ijkm} are mutually independent random variables. The term α_i represents the expected difference between the output simulated by model structure *i*

and the mean μ, over all parameter sets, input levels and internal variability. The variance of α_i is the variance due to structure uncertainty. Similarly, the interpretation of terms β_j , γ_k , δ_{jk} and ε_{ijkm} can be obtained. Detailed information is listed in Table 3, and in the calculations, the bar denotes averaging and the dots indicate which component has been averaged over.

<Table 3>

Following the style of Northrop and Chandler (2014), finite-populations and superpopulations denote sampling space under finite case and probability case, respectively. In practice, the variances from finite-populations were written as $(U_S^2, U_P^2, U_I^2, U_{PI}^2, U_v^2)$, while variances from superpopulations in Bayesian inference were called $(\sigma_S^2, \sigma_P^2, \sigma_I^2, \sigma_{PI}^2, \sigma_v^2)$, in order to distinguish the respective cases.

In Bayesian inference, our preliminary interest focused on estimating the parameter $\theta = (\sigma_S, \sigma_P, \sigma_I, \sigma_{PI}, \sigma_v)$. The Bayesian law can be given by:

$$L(\theta \mid \tilde{y}) = \frac{L(\theta)\,\mathrm{L}(\tilde{y} \mid \theta)}{\mathrm{L}(\tilde{y})} \tag{8}$$

where $L(\theta)$ denotes the prior distribution; $\mathrm{L}(\tilde{y} \mid \theta)$ is the likelihood function, a function of θ; and $\mathrm{L}(\tilde{y})$ denotes the evidence. Because the relative posterior $L(\theta \mid \tilde{y})$ of parameters is independent of $\mathrm{L}(\tilde{y})$, it can be conveniently removed from the denominator. Then, the posterior is proportional to $L(\theta)\,\mathrm{L}(\tilde{y} \mid \theta)$. In the Bayesian approach, α_i, differences in model structure are handled as independent, identically distributed normal random variables with zero mean and σ_S^2 variance, i.e. $\alpha_i \sim N(0, \sigma_S^2)$. And similar notations for β_j, γ_k, δ_{jk} and ε_{ijkm} can be written as $\beta_j \sim N(0, \sigma_P^2)$, $\gamma_k \sim N(0, \sigma_I^2)$, $\delta_{jk} \sim N(0, \sigma_{PI}^2)$, and $\varepsilon_{ijkm} \sim N(0, \sigma_v^2)$, respectively.

A primary step of the Bayesian implementation is to define the form of prior belief of parameters, derived from existing information. Commonly used prior distributions include the vague non-informative prior, normal distribution, Beta distribution and inverse-Gamma distribution (Jarraya et al., 2014). However, in the case of limited data length, the information provided by existing data is very little, frequently resulting in distorted inferences owing to an abnormally high density of probability near zero. Therefore, we derived prior from the half-Cauchy distribution, whose appealing feature is that it only provides a weak prior and encapsulates some basic constraints on parameters, instead of concentrating more of prior close to zero (Gelman, 2006). Half-Cauchy distribution follows the probability density form of:

$$p(\sigma) = \frac{2}{\pi \times A \times (1 + \frac{\sigma^2}{A^2})} \tag{9}$$

By controlling the scale parameter *A*, the prior mass of standard deviations in superpopulation can range over a plausible interval. At the present context, as a rule of thumb, *A* is roughly set to one-quarter of the prior range (for details of *A*, see Fig. 9).

The realization of Bayesian sampling depends on the DiffeRential Evolution Adaptive Metropolis (DREAM) method, using Markov Chain Monte Carlo (MCMC) as its main building block (Joseph and Guillaume, 2013; Vrugt and Ter Braak, 2011; Yang et al., 2008), via R package "dream" (Joseph and Guillaume, 2013). This ensures that multiple parameter sets can be evaluated simultaneously and a spectacular reduction in time is obtained due to the parallel strategy. The DREAM algorithm, which runs multiple Markov chains in parallel and automatically adjusts the scale, explores the posterior target distribution before converging to a limiting distribution. The DREAM method is recommended for its attempt to disentangle the contribution of input, parameter and model structure uncertainty to total model uncertainty in our case study (Vrugt and Robinson, 2007; Vrugt et al., 2009).

For comparing the difference of each uncertainty source among individual configuration schemes, Bayesian inference was also employed to obtain the medians and 75%/95% percentiles of simulated streamflow and three N loadings, based on the ensemble output derived from ANOVA. The method used here is the same as above, i.e. Eqs. (6)-(7) and DREAM algorithm.

<Fig. 3>

4. Results

4.1 Total uncertainty in predicting streamflow and N loadings

Fig. 4 presents the medians and 95% confidence intervals of predicted daily mean streamflow and watershed-averaged loadings of three N species using the BayeANOVA method, demonstrating larger prediction uncertainty of simulated high values than that of low values, especially for NO_3^--N and TN. Simulated streamflow and N loadings showed a distinct seasonal variation across the 3-year study period.

<Fig. 4>

The observed values of streamflow and N loadings are also presented in Fig. 4. Almost all observation data of streamflow followed the median curve and were within the 95% confidence intervals, indicating good performance of the model. The performance of simulated N loadings was not as good as that of streamflow. As described in Fig. 4b, a small part of observed NH_4^+-N loadings could not be captured accurately, mainly in the first year. Compared to the simulated NH_4^+-N loading, the modeling of NO_3^--N and TN loadings was much better, since more observation data were overlapped by the uncertainty band. For the three N loadings, the outliers were primarily distributed in the extreme areas, suggesting that improving simulation of extreme values has significant importance for watershed N modeling.

4.2 Comparison of multi-source uncertainties

To comprehensively assess the timing and magnitude of individual multi-source uncertainties as well as the relative contributions to the total uncertainty in simulating streamflow and N loadings, we quantified the individual variances corresponding to five uncertainty sources and their fractional proportions using ANOVA. Since we did not distinguish the concepts of uncertainty and variability, the variance in each source acted as an available alternative to the uncertainty.

4.2.1 Relative contribution of five sources of uncertainty

Among the five sources, the precipitation input uncertainty resulted in the greatest uncertainty in simulating streamflow, with its variance ranging from nearly 0 to 20.3 $(m^3\ s^{-1})^2$ over the study period (Fig. 5). Conversely, the model structure uncertainty had nearly no influence on streamflow formation, with variance of approximately 0 $(m^3/s)^2$. The uncertainty linked to parameters was slightly lower than that to inputs, in most cases. Uncertainties generated from the interaction effects and internal variability were relatively small when compared to that from inputs and parameters.

<Fig. 5>

In the three N loading simulations, parameter uncertainty contributed the greatest fractional proportion of total uncertainty over the three-year average period, with fraction values of 58.83%, 63.48% and 61.64% for NH_4^+-N, NO_3^--N and TN loading, respectively (Figs. 6, 7 and 8). The second contributor to total uncertainty was input uncertainty, with fraction values of 31.49%, 18.04% and 22.51%, respectively.

<Fig. 6>

Furthermore, from the fractional variances in Figs. 5b, 6b, 7b and 8b, it was apparent that the interaction effects between parameters and inputs were very comparable in timing and magnitude among simulated streamflow and three N

loadings (the average contribution approximately ranged from 6.12% to 8.47%, Table 4). This suggests a steady contribution of the uncertainty arising from interaction effects to the total uncertainty. Contrary to streamflow, structure uncertainty in modeling three N loadings was obvious, especially for the case of NO_3^--N loading. A feature of internal variability should be noted: the internal variability of N loadings exhibited a disproportionately great influence on total uncertainty in the first six months, compared to the later period. Although each CNMM run was allotted a relatively long "warm-up" period of ten months before stepping into the study period, the random errors generated from the model itself in the first few months still produced non-negligible uncertainty. Shorter "warm-up" periods have been explored (not shown here); however, the results from these studies gave even larger internal variability. This suggests that a suitable "warm-up" period plays a significant role in enhancing the modeling ability, since the inherent uncertainty in environmental system is uncontrollable.

<Fig. 7>

<Fig. 8>

4.2.2 Comparison of uncertainties in the rice-growing season and fallow season

Comparisons of multi-source uncertainties in the rice-growing season against fallow season were carried out (Figs. 5a, 6a, 7a, 8a and Table 4), and contrasting results were obtained. The total uncertainty of simulated streamflow averaged across three years was larger in the fallow season (2.04 $(m^3\ s^{-1})^2$) than that in the rice-growing season (1.52 $(m^3\ s^{-1})^2$) (gray band in Fig. 5a).

Unlike the case of uncertainty in streamflow simulation, three of the largest uncertainty components (i.e. parameters, inputs and interaction effects) among the five sources and the total uncertainty of three simulated N loadings were, on average,

significantly greater in the rice-growing season than those in the fallow season (Table 4). Take TN loading for example, the uncertainties related to parameters, inputs, interaction effects and total uncertainty were 3.31, 1.07, 0.32 and 4.86 (kg km^{-2} d^{-1})^2 respectively, in the rice-growing season, which were greater than those in the fallow season (with values of 2.75, 0.55, 0.16 and 3.81 (kg km^{-2} d^{-1})^2, respectively). Specifically, the peaks of multi-source uncertainties in all three N loadings occurred in the rice-growing season for the first two years, although in 2013 the peak values of uncertainty components did not occur during the rice-growing season. Both the average uncertainty components across three years and those in 2012-2013 were much larger in the rice-growing season than that in the fallow season. The magnitude of multi-source uncertainties among three N loading simulations in the rice-growing season showed great differences. For instance, the averaged multi-source uncertainties of simulated NH_4^+-N loading were smallest, with the maximum component of 0.25 (kg km^{-2} d^{-1})^2 in parameter uncertainty, while the simulated TN loading uncertainties were the largest, with the maximum component of 3.31 (kg km^{-2} d^{-1})^2 in parameter uncertainty. In addition, in the simulated TN loading uncertainty, the NO_3^--N fraction contributed a dominant proportion (75.48%), compared to that from NH_4^+-N.

<Table 4>

4.3 Bayesian estimation of multi-source uncertainties

After the multi-source uncertainties were partitioned chronologically for simulated streamflow and N loadings, the Bayesian technique was applied to estimate the standard deviations of sampling from a superpopulation under the stochastic framework.

First, Fig. 9 illustrates the posterior distributions of standard deviations related to the five sources of uncertainty, with the prior distributions plotted as red lines. It is

worth noting that the prior lines were virtually flat except for the interaction effects σ_{PI} of streamflow, implying the prior weakly restricted the likelihood values. As anticipated in section 3.3, for parameters $\sigma_o, \sigma_s, \sigma_p$ and σ_v, the information derived from the likelihood functions dominated the formation of posterior distributions. In general, the half-Cauchy prior distribution had an expected robust behavior on the Bayesian posterior estimation.

<Fig. 9>

Then, a comparison of inter-category difference between a specific uncertainty source from the model structures, parameters or inputs, was conducted in the rice-growing season and compared against the fallow season. The posterior statistics (median values, 25th-75th and 5th-95th percentiles) of prediction results from an individual model solution can provide more details on different levels of each uncertainty source. The predicted streamflow medians non-uniformly increased with increasing precipitation inputs to CNMM, along with higher 75th/95th percentiles in the fallow season, relative to the rice-growing season (Fig. 10a). The medians of simulated N loadings did not always increase with increasing precipitation, suggesting nonlinearity between change in N loading and change in precipitation. Under different precipitation input levels, although the medians of simulated N loadings were comparable between the two seasons, the uncertainty ranges (25th-75th and 5th-95th percentiles) were apparently larger in the rice-growing season when compared with the fallow season.

Fig. 10b shows the change of model structures had little impact on streamflow simulation, while it induced an apparent change in N loading modeling. Notably, the basic model (S1) produced minimal simulation error in all three N loadings, demonstrating that the initial structure, i.e., S1 of CNMM, with relatively complete N

processes can give better performance. In most cases, the 75th/95th percentiles of N loadings in the rice-growing season were slightly higher than those in the fallow season.

<Fig. 10>

H1, H2 and H3 denote half of optimal set, optimal set and twofold optimal set of hydrologic parameters, respectively, and N1, N2 and N3 represent the same meaning of N parameters (Fig. 10c). The increase in parameter set from H2 to H3 caused an extreme decrease in both median and 75th/95th percentiles of simulated streamflow. The change in N parameters (from N1 to N3) led to a slight change in 95th percentiles of the streamflow, despite the unaffected medians. Both medians and 75th/95th percentiles of three simulated N loadings with H1 decreased, while those with H3 dramatically increased, compared to those with optimal set, H2. The increase from N1 to N3 resulted in increasing median and 75th/95th percentiles of NO_3^--N loading, without an observed uniform trend for NH_4^+-N or TN loading.

5 Discussion

5.1 Main factors controlling multi-source uncertainties in N loading simulation

Failure to identify major sources of uncertainty in simulating watershed behavior is known to bias model prediction (Ajami et al., 2007; Yen et al., 2014), but the main contributor to multi-source uncertainties in simulating N dynamics at watershed scale remains largely unknown. Consistent with previous modeling studies on several environmental constituents (N and phosphorus loadings: Shen et al., 2013; pesticide leaching: Steffens et al., 2013; streamflow: Tian et al., 2014), parameter uncertainty dominantly controlled the total uncertainty in N loading simulations in the present study. This phenomenon was attributed to the heterogeneity of stream N and nonlinearity of the distributed hydrologic nutrient model, thus leading to high

sensitivity of predicted stream water N loadings to the selected parameters. Another feature of parameter uncertainty found in this study revealed that streamflow and N loading simulations could be controlled by both hydrologic and N process parameters (Fig. 10). This suggests that the quantity and quality of water should be given equal importance, rather than separately calibrating their modeling effects in uncertainty analysis, as is commonly practiced. Zhang et al. (2016) provided a similar recommendation for considering high interactions of runoff and NH_4^+-N concentration prediction in an integrated water system model using a combined auto-calibration multi-process approach. The stream water N loading prediction was highly constrained by parameter uncertainty, indicating the importance of optimizing the parameter set, while other sources of uncertainty also augment the total uncertainty.

The primary purpose of model uncertainty analysis is to control and further reduce the uncertainty, mainly focusing on anthropogenic epistemic uncertainties (Li, 2012). However, the distributed hydrologic-water quality models (e.g. CNMM) are time-consuming tools with high computational complexity. Therefore, allocating limited computational resources to obtain optimal precision is challenging when confronting the uncertainties that arise from model structures, parameter sets, inputs and other potential sources. One possible route, provided in our study, would be to use a weighting scheme according to the contribution of different uncertainty sources in statistical models related to scientific questions. Therefore, when simulating streamflow, the precision of input data should be improved, since precipitation input uncertainty is the main source of significant degree of uncertainty. Given the important role of parameter uncertainty, as the largest source of uncertainty in simulating N loadings, parameter identification should be given particular attention.

5.2 Increased uncertainty and pollution risk resulting from rice agriculture

The large uncertainty in modeling N loadings in the present study was probably linked to human activities in the Tuojia watershed. According to previous studies in this study area (Li et al., 2015; Wang et al., 2014), high values of N loadings in stream water are induced by large applications of N fertilizer and herbicide to paddy fields during the rice-growing season for yield improvement purpose. Fertilizer utility directly increases N input to the watershed, while herbicide decreases the N uptake of plants by killing weeds indirectly, resulting in more N leaching into subsoil. In our study, three of the largest uncertainty components (i.e. parameters, inputs and interaction effects) and total uncertainty in all three simulated N loadings increased dramatically in magnitude over the course of three years during the rice-growing season when compared to the fallow season (Table 4). This indicates that high loadings of N and large uncertainties were largely induced by rice cropping in the Tuojia watershed. Specifically, agricultural management practice (especially for the input of excessive fertilization) conducted during the rice-growing season leads to the acceleration of N cycle and more residual N transported into stream water. This management practice and resulting high N loadings cause more difficulties in predicting N loading and larger uncertainties in N modeling.

As highly vulnerable regions regarding non-point source pollution, rice agricultural watersheds are predicted to export large proportions of N (Shi et al., 2010; Wang et al., 2015). Reducing N input to the watershed by making a balance between socioeconomic performance and affordable environmental pollution risk is the fundamental solution for reducing N loading levels and predicting uncertainty. As shown in Fig. 11, the cumulative probability curve exhibits a risk assessment of estimated TN loading. The predicted medians of TN loading were 2.87 and 3.04 kg

km^{-2} d^{-1} in the fallow season and the rice-growing season, respectively, with corresponding cumulative probabilities of 0.66 and 0.70. In the context of the Tuojia watershed, the theoretically reasonable value of TN loading is approximately 1.41 kg km^{-2} d^{-1}, according to the national standard level (1.0 mg L^{-1}). Thus, the predicted TN loadings in both seasons significantly exceeded the standard range. Compared to the fallow season, the TN loading in the rice-growing season poses a more severe threat to the healthy water environment. The averaged risk probability should be reduced to 0.37 and 0.46 in the fallow season and rice-growing season, respectively, to achieve the design objective when taking 1 kg km^{-2} d^{-1} of TN as the baseline for required loading reduction. Practical design experiments need to include more complex information, such as social and natural demands, and the risk probability depends on the specific model and watershed conditions (Chen et al., 2012; Liang et al., 2016; Nearing and Gupta, 2015). Nevertheless, the risk estimation approach, in our case, can be explored to support decision making and planning in agricultural management practices.

<Fig. 11>

Both the multi-source uncertainty components and the total uncertainty of NO_3^--N loading were larger than those of NH_4^+-N loading (Figs. 6 and 7). The simulated NO_3^--N loading contributed to 74.50%, 69.82%, 76.38% and 75.48% in the parameter uncertainty, input uncertainty, interaction effects and total uncertainty of simulated TN, respectively. However, from the observation data of NH_4^+-N, NO_3^--N and TN loadings during the study period (Fig. 4), it appears that the proportion of NO_3^--N to TN loading (39.45%) was similar to that of NH_4^+-N to TN (34.44%). Therefore, NO_3^--N loading contributed a high percentage of the total uncertainty of TN loading simulation, and this percentage was disproportionate with the ratio of

observed NO_3^--N to TN loading. The significant contribution of NO_3^--N simulation uncertainty to TN simulation uncertainty could be attributed to the tendency of simulated soil NO_3^--N leaching, resulting from paddy tillage and subsoil properties (such as texture, bulk density or negatively charged soil particles) (Klatt et al., 2016; Wang et al., 2014). The inaccuracy of NO_3^--N loading prediction was the dominant cause of the large uncertainty of TN loading.

Consequently, summarizing the above discussion of uncertainty in CNMM and the risk assessment in practical decision-making, it can be concluded that reducing the parameter uncertainty of NO_3^--N loading simulation during the rice-growing season is the key factor to improving N modeling precision in rice agricultural watersheds. This conclusion can be extended to other similar regions or watersheds with more detailed configuration and implementation of the BayeANOVA method for allowable loading calculation and margin of safety determination in agricultural practice and environment managements.

6 Conclusion

This study employed Bayesian inference combined with ANOVA to partition the prediction uncertainty of stream water N loadings into five uncertainty sources. The comparison of relative contributions of individual uncertainty sources to the total uncertainty showed that in the three N loading simulations, parameter uncertainty was the greatest factor inducing uncertainty, while the second was generated from precipitation input. Three of the largest uncertainties (i.e. parameters, inputs and interaction effects) in all three simulated N loadings, were on average significantly greater during the rice-growing seasons when compared to the fallow seasons. This was primarily due to the excess fertilization application during the rice-growing seasons. The simulated NO_3^--N loading, contributing to 75.48% of total uncertainty,

was found to be more inaccurate when compared to the NH_4^+-N loading. Therefore, the parameter uncertainty in NO_3^--N loading prediction during the rice-growing season was considerable, and it was the essential problem of N modeling in rice agricultural watershed.

The BayeANOVA approach can be extended to other studies associated with multi-source uncertainty analysis. The risk assessment of N pollution in our study can provide scientific and technological support for N pollution control and management of similar agricultural watersheds.

Acknowledgements

The authors appreciate the staff of Institute of Subtropical Agriculture, Chinese Academy of Sciences for providing meteorological, hydrologic and water quality data. This study was financially supported by the National Natural Science Foundation of China (grant numbers: 51525902 and 51479139) as well as by the "Hundred Talent Program of the Chinese Academy of Sciences" (Granted to Dr. Siyue Li). Appreciation is also extended to the editors and the anonymous reviewers for their comments and suggestions.

References:

Ahn, K., Merwade, V., Ojha, C. and Palmer, R.N., 2016. Quantifying relative uncertainties in the detection and attribution of human-induced climate change on winter streamflow. J. Hydrol., 542: 304-316.

Ajami, N.K., Duan, Q. and Sorooshian, S., 2007. An integrated hydrologic Bayesian multimodel combination framework: Confronting input, parameter, and model structural uncertainty in hydrologic prediction. Water Resour. Res., 43(1).

Alexander, R.B., Johnes, P.J., Boyer, E.W. and Smith, R.A., 2002. A comparison of models for estimating the riverine export of nitrogen from large watersheds. Biogeochemistry, 57/58: 295-339.

Arabi, M., Govindaraju, R.S. and Hantush, M.M., 2007. A probabilistic approach for analysis of uncertainty in the evaluation of watershed management practices. J. Hydrol., 333(2): 459-471.

Arabi, M., Govindaraju, R.S., Engel, B. and Hantush, M., 2007. Multiobjective sensitivity analysis of sediment and nitrogen processes with a watershed model. Water Resour. Res., 43: W06409.

Arhonditsis, G.B., Perhar, G., Zhang, W., Massos, E., Shi, M. and Das, A., 2008. Addressing equifinality and uncertainty in eutrophication models. Water Resour. Res., 44: W01420.

Bardule, A., Grinfelde, I., Lazdina, D., Bardulis, A. and Sarkanabols, T., 2017. Macronutrient leaching in a fertilized juvenile hybrid aspen (Populus tremula L. × P. tremuloides Michx.) plantation cultivated in an agroforestry system in Latvia. Hydrol. Res.(in press).

Beven, K., 1993. Prophecy, reality and uncertainty in distributed hydrological modelling. Adv. Water Resour., 16(1): 41-51.

Beven, K., 2006. A manifesto for the equifinality thesis. J. Hydrol., 320(1): 18-36.

Bhowmik, A.K. and Costa, A.C., 2015. Representativeness impacts on accuracy and precision of climate spatial interpolation in data‐scarce regions. Meteorol. Appl., 22(3): 368-377.

Bosch, N.S., 2008. The influence of impoundments on riverine nutrient transport: An evaluation using the Soil and Water Assessment Tool. J. Hydrol., 355(1): 131-147.

Bouman, B., Humphreys, E., Tuong, T.P. and Barker, R., 2007. Rice and water. Adv. Agron., 92: 187-237.

Bouraoui, F. and Grizzetti, B., 2014. Modelling mitigation options to reduce diffuse nitrogen water pollution from agriculture. Sci. Total Environ., 468: 1267-1277.

Brown, L.C. and Barnwell, T.O., 1987. The enhanced stream water quality models QUAL2E and QUAL2E-UNCAS: documentation and user manual. US Environmental Protection Agency. Office of Research and Development. Environmental Research Laboratory.

Chebana, F., Dabo Niang, S. and Ouarda, T.B., 2012. Exploratory functional flood frequency analysis and outlier detection. Water Resour. Res., 48(4).

Chen, D., Dahlgren, R.A., Shen, Y. and Lu, J., 2012. A Bayesian approach for calculating variable total maximum daily loads and uncertainty assessment. Sci. Total Environ., 430: 59-67.

Chen, D., Hu, M. and Dahlgren, R.A., 2014. A dynamic watershed model for determining the effects of transient storage on nitrogen export to rivers. Water Resour. Res., 50(10): 7714-7730.

Du, Z., Zhou, X., Shao, J., Yu, G., Wang, H., Zhai, D., Xia, J. and Luo, Y., 2017. Quantifying uncertainties from additional nitrogen data and processes in a terrestrial ecosystem model with Bayesian probabilistic inversion. J. Adv. Model. Earth Sy., 09.

Duan, Q., Schaake, J., Andreassian, V., Franks, S., Goteti, G., Gupta, H.V., Gusev, Y.M., Habets, F., Hall, A. and Hay, L., 2006. Model Parameter Estimation Experiment (MOPEX): An overview of science strategy and major results from the second and third workshops. J. Hydrol., 320(1): 3-17.

Eshleman, K.N., Sabo, R.D. and Kline, K.M., 2013. Surface water quality is improving due to declining

atmospheric N deposition. Environ. Sci. Technol., 47(21): 12193-12200.

Gao, Y., Zhu, B., Yu, G., Chen, W., He, N., Wang, T. and Miao, C., 2014. Coupled effects of biogeochemical and hydrological processes on C, N, and P export during extreme rainfall events in a purple soil watershed in southwestern China. J. Hydrol., 511: 692-702.

Gardner, K.K., McGlynn, B.L. and Marshall, L.A., 2011. Quantifying watershed sensitivity to spatially variable N loading and the relative importance of watershed N retention mechanisms. Water Resour. Res., 47: W08524.

Gelman, A., 2006. Prior distributions for variance parameters in hierarchical models (comment on article by Browne and Draper). Bayesian Anal., 1(3): 515-534.

Hamilton, S.K., 2012. Biogeochemical time lags may delay responses of streams to ecological restoration. Freshwater Biol., 57(s1): 43-57.

Harmel, R.D. and Smith, P.K., 2007. Consideration of measurement uncertainty in the evaluation of goodness-of-fit in hydrologic and water quality modeling. J. Hydrol., 337(3): 326-336.

Harmel, R.D., Cooper, R.J., Slade, R.M., Haney, R.L. and Arnold, J.G., 2006. Cumulative uncertainty in measured streamflow and water quality data for small watersheds. Am. Soc. Agr. Eng., 49(3): 689.

Hawkins, E. and Sutton, R., 2009. The potential to narrow uncertainty in regional climate predictions. B. Am. Meteorol. Soc., 90(8): 1095-1107.

Hawkins, E. and Sutton, R., 2011. The potential to narrow uncertainty in projections of regional precipitation change. Clim. Dynam., 37(1-2): 407-418.

Hill, T., Lewicki, P. and Lewicki, P., 2006. Statistics: methods and applications: a comprehensive reference for science, industry, and data mining. StatSoft, Inc.

Hrachowitz, M., Savenije, H., Blöschl, G., McDonnell, J.J., Sivapalan, M., Pomeroy, J.W., Arheimer, B., Blume, T., Clark, M.P. and Ehret, U., 2013. A decade of Predictions in Ungauged Basins (PUB)—a review. J. Hydrol. Sci., 58(6): 1198-1255.

Jarraya, A., Leray, P. and Masmoudi, A., 2014. Implicit parameter estimation for conditional gaussian bayesian networks. Int. J. Comput. Int. Sys., 7(sup1): 6-17.

Jiang, S., Jomaa, S., Büttner, O., Meon, G. and Rode, M., 2015. Multi-site identification of a distributed hydrological nitrogen model using Bayesian uncertainty analysis. J. Hydrol., 529(2015): 940-950.

Joseph, J.F. and Guillaume, J.H.A., 2013. Using a parallelized MCMC algorithm in R to identify appropriate likelihood functions for SWAT. Environ. Modell. Softw., 46: 292-298.

Klatt, S., Kraus, D., Rahn, K., Werner, C., Kiese, R., Butterbach-Bahl, K. and Haas, E., 2016. Parameter-Induced Uncertainty Quantification of Regional N O Emissions and NO Leaching using the Biogeochemical Model LandscapeDNDC. Synthesis and Modeling of Greenhouse Gas Emissions and Carbon Storage in Agricultural and Forest Systems to Guide Mitigation and Adaptation(advagricsystmodel6): 149-172.

Krupa, M., Tate, K.W., van Kessel, C., Sarwar, N. and Linquist, B.A., 2011. Water quality in rice-growing watersheds in a Mediterranean climate. Agric Ecosyst Environ, 144(1): 290-301.

Kudo, R., Yoshida, T. and Masumoto, T., 2017. Uncertainty analysis of impacts of climate change on snow processes: Case study of interactions of GCM uncertainty and an impact model. J. Hydrol., 548: 196-207.

Li, M., 2012. Uncertainty estimation of hydrological models under a Bayesian framework, Ph. D dissertation. Tsinghua University.

Li, Y., Jiao, J., Wang, Y., Yang, W., Meng, C., Li, B., Li, Y. and Wu, J., 2015. Characteristics of nitrogen loading and its influencing factors in several typical agricultural watersheds of subtropical China. Environ. Sci. Pollut. R., 22(3): 1831-1840.

Li, Y., Li, Y. and Wang, Y., 2017. CNMM: a grid-based spatially-distributed catchment simulation model. China Science Press, Beijing, China, 221 pp.

Li, Y., White, R., Chen, D., Zhang, J., Li, B., Zhang, Y., Huang, Y. and Edis, R., 2007. A spatially referenced water and nitrogen management model (WNMM) for (irrigated) intensive cropping systems in the North China Plain. Ecol. Model., 203(3-4): 395-423.

Liang, S., Jia, H., Xu, C., Xu, T. and Melching, C., 2016. A Bayesian approach for evaluation of the effect of water quality model parameter uncertainty on TMDLs: A case study of Miyun Reservoir. Sci. Total Environ., 560: 44-54.

Lindenschmidt, K., Fleischbein, K. and Baborowski, M., 2007. Structural uncertainty in a river water quality modelling system. Ecol. Model., 204(3-4): 289-300.

Lovenduski, N.S., McKinley, G.A., Fay, A.R., Lindsay, K. and Long, M.C., 2016. Partitioning uncertainty in ocean carbon uptake projections: Internal variability, emission scenario, and model structure. Global Biogeochem. Cy., 30(9): 1276-1287.

McIntyre, N.R. and Wheater, H.S., 2004. Calibration of an in-river phosphorus model: prior evaluation of data needs and model uncertainty. J. Hydrol., 290(1): 100-116.

Nearing, G.S. and Gupta, H.V., 2015. The quantity and quality of information in hydrologic models. Water Resour. Res., 51(1): 524-538.

Northrop, P.J. and Chandler, R.E., 2014. Quantifying sources of uncertainty in projections of future climate. J. Climate, 27(23): 8793-8808.

Qian, F., Huang, J., Liu, J. and Liu, H., 2017. Effects of flow hydraulics on total nitrogen loss on steep slopes under simulated rainfall conditions. Hydrol. Res.: nh2017261.

Shen, Z., Chen, L., Hong, Q., Qiu, J., Xie, H. and Liu, R., 2013. Assessment of nitrogen and phosphorus loads and causal factors from different land use and soil types in the Three Gorges Reservoir Area. Sci. Total Environ., 454: 383-392.

Shi, L., Ji, X. and Li, H., 2010. Nitrogen and phosphorous losses from surface runoff under different application in the double cropping rice field in Hunan., Chinese J. Agrometeor. (in Chinese), pp. 551-557.

Shields, C.A. and Tague, C.L., 2012. Assessing the role of parameter and input uncertainty in ecohydrologic modeling: implications for a semi-arid and urbanizing coastal California catchment, Ecosystems, pp. 775-791.

Steffens, K., Larsbo, M., Moeys, J., Jarvis, N. and Lewan, E., 2013. Predicting pesticide leaching under climate change: Importance of model structure and parameter uncertainty. Agric. Ecosyst. Environ, 172: 24-34.

Sullivan, T.J., Cosby, B.J., Herlihy, A.T., Webb, J.R., Bulger, A.J., Snyder, K.U., Brewer, P.F., Gilbert, E.H. and Moore, D.L., 2004. Regional model projections of future effects of sulfur and nitrogen deposition on streams in the southern Appalachian Mountains. Water Resour. Res., 40: W02101.

Tian, Y., Booij, M.J. and Xu, Y.P., 2014. Uncertainty in high and low flows due to model structure and parameter errors. Stoch. Env. Res. Risk a., 28(2): 319-332.

Uniyal, B., Jha, M.K. and Verma, A.K., 2015. Parameter identification and uncertainty analysis for simulating streamflow in a river basin of Eastern India. Hydrol. Process., 29(17): 3744-3766.

Valipour, M., Banihabib, M.E. and Behbahani, S.M.R., 2013. Comparison of the ARMA, ARIMA, and the autoregressive artificial neural network models in forecasting the monthly inflow of Dez dam reservoir. J. Hydrol., 476: 433-441.

Vrugt, J.A. and Robinson, B.A., 2007. Treatment of uncertainty using ensemble methods: Comparison of sequential data assimilation and Bayesian model averaging. Water Resour. Res., 43(1): W01411.

Vrugt, J.A. and Ter Braak, C.J., 2011. DREAM (D): an adaptive Markov Chain Monte Carlo simulation algorithm to solve discrete, noncontinuous, and combinatorial posterior parameter estimation problems. Hydrol. Earth Syst. Sc., 15(12): 3701-3713.

Vrugt, J.A., Ter Braak, C.J., Gupta, H.V. and Robinson, B.A., 2009. Equifinality of formal (DREAM) and

informal (GLUE) Bayesian approaches in hydrologic modeling? Stoch. Env. Res. Risk a., 23(7): 1011-1026.

Wang, A., Tang, L. and Yang, D., 2016. Spatial and temporal variability of nitrogen load from catchment and retention along a river network: a case study in the upper Xin'anjiang catchment of China. Hydrol. Res., 47(4): 869-887.

Wang, Y., Li, Y., Liu, F., Li, Y., Song, L., Li, H., Meng, C. and Wu, J., 2014. Linking rice agriculture to nutrient chemical composition, concentration and mass flux in catchment streams in subtropical central China. Agric. Ecosyst. Environ., 184: 9-20.

Wang, Y., Liu, X., Li, Y., Liu, F., Shen, J., Li, Y., Ma, Q., Yin, J. and Wu, J., 2015. Rice agriculture increases base flow contribution to catchment nitrate loading in subtropical central China. Agriculture, Ecosystems & Environment, 214: 86-95.

Wellen, C., Kamran-Disfani, A. and Arhonditsis, G.B., 2015. Evaluation of the current state of distributed watershed nutrient water quality modeling. Environ. Sci. Technol., 49(6): 3278-3290.

Yang, H., Yang, J., Reichert, P., Abbaspour, K.C. and Xia, J., 2008. Comparing uncertainty analysis techniques for a SWAT application to the Chaohe Basin in China. J. Hydrol., 358(1): 1 - 23.

Yen, H., Wang, X., Fontane, D.G., Harmel, R.D. and Arabi, M., 2014. A framework for propagation of uncertainty contributed by parameterization, input data, model structure, and calibration/validation data in watershed modeling. Environ. Modell. Softw., 54: 211-221.

Yip, S., Ferro, C.A., Stephenson, D.B. and Hawkins, E., 2011. A simple, coherent framework for partitioning uncertainty in climate predictions. J. Climate, 24(17): 4634-4643.

Young, P.C. and Parkinson, S., 2002. Simplicity out of complexity. Developments in Environmental Modelling, 22: 251-301.

Zhang, Y., Shao, Q. and Taylor, J.A., 2016. A balanced calibration of water quantity and quality by multi-objective optimization for integrated water system model. J. Hydrol., 538(2016): 802-816.

Table 1. Brief attributes of key parameters controlling nitrogen transformation and hydrologic process.

Parameter	Physical meaning	Unit	Range	Optimal
Hydrologic parameters				
phy_fc	Field capacity	%	0.078-0.708	grid-based
phy_ks	Soil vertical hydraulic conductivity	m d^{-1}	0.001-9.972	grid-based
phy_kslat	Soil lateral hydraulic conductivity	m d^{-1}	0.000-4.986	grid-based
manning	The manning roughness coefficient	-	0.010-0.700	channel segment-based
Nitrogen-process parameters				
half_satu	Michaelis-menton half-saturation constant for N	mg L^{-1}	0.010-0.300	0.015
mu_max	Maximum specific algal growth rate at 20℃	1 d^{-1}	0-10	1
p_n	Algal preference factor for ammonium	-	0-1	0.150
bc1	Rate constant for biological oxidation of NH_4^+-N to NO_2^--N in stream at 20℃	1 d^{-1}	0-5	0.050
bc2	Rate constant for biological oxidation of NO_2^--N to NO_3^--N in stream at 20℃	1 d^{-1}	0-5	0.200
bc3	Rate constant for denitrification in stream at 20℃	1 d^{-1}	0-100	15

Table 2. Configuration information of CNMM in different precipitation inputs, model structures and parameter sets.

Precipitation input	
Level	Description
L1	L-50%L
L2	L-30%L
L3	L-10%L
L4	L
L5	L+10%L
L6	L+30%L
L7	L+50%L
Model structure	
Version	Description
S1	CNMM
S2	CNMM without N uptake function by plant
S3	CNMM with temperature-constant coefficient
Parameter set	
Classification	Description
H1	0.5Par
H2	Par
H3	2.0Par
N1	0.5Par
N2	Par
N3	2.0Par

L: precipitation series of measurements; H: hydrologic parameters; N: nitrogen parameters; Par: optimal parameter sets.

Table 3. Decomposition of total uncertainty into components in ANOVA.

Sources of uncertainty	Difference/Variance	Expression
Model structure (S)	Difference	$\hat{\alpha}_i = \bar{Y}_{i\ldots} - \bar{Y}_{\ldots\ldots}$
	Variance	$U_S^2 = \frac{1}{N_S - 1}\sum_i (\hat{\alpha}_i - \bar{\alpha})^2$
Parameter set (P)	Difference	$\hat{\beta}_j = \bar{Y}_{.j..} - \bar{Y}_{\ldots\ldots}$
	Variance	$U_P^2 = \frac{1}{N_P - 1}\sum_j (\hat{\beta}_j - \bar{\beta})^2$
Precipitation input (I)	Difference	$\hat{\gamma}_k = \bar{Y}_{..k.} - \bar{Y}_{\ldots\ldots}$
	Variance	$U_I^2 = \frac{1}{N_I - 1}\sum_k (\hat{\gamma}_k - \bar{\gamma})^2$
Interaction effect (PI)	Difference	$\hat{\delta}_{jk} = \bar{Y}_{.jk.} - \bar{Y}_{.j..} - \bar{Y}_{..k.} + \bar{Y}_{\ldots\ldots}$
	Variance	$U_{PI}^2 = \frac{1}{(N_P - 1)(N_I - 1)}\sum_{jk} (\hat{\delta}_{jk} - \bar{\delta})^2$
Internal variability (v)	Difference	$\hat{\varepsilon}_{ijkm} = Y_{ijkm} - \bar{Y}_{ijk.}$
	Variance	$U_v^2 = \frac{1}{(N_S - 1)(N_P - 1)(N_I - 1)(N_M - 1)}\sum_{ijkm} (\hat{\varepsilon}_{ijkm} - \bar{\varepsilon})^2$

A bar denotes averaging and the dots indicate which component has been averaged over. N_M denotes the average number of repeated model runs generating uncertainty in internal variability.

Table 4. Summary of the averaged variances and fractional variances in ANOVA.

	Sources of uncertainty	Min	Max	Mean			Fraction %
		Streamflow: $(m^3\ s^{-1})^2$/N loading: $(kg\ km^{-2}\ d^{-1})^2$					
				Fallow season	Rice-growing season	Average	
Streamflow	U_I^2	5.93E-04	20.33	1.22	0.84	1.04	60.96
	U_S^2	5.67E-12	2.51E-04	7.82E-06	2.65E-05	1.73E-05	2.66E-03
	U_P^2	0.15	14.74	0.73	0.54	0.63	30.10
	U_{PI}^2	0.00	0.86	0.09	0.15	0.12	8.47
	U_v^2	6.10E-07	3.56E-02	6.65E-04	1.60E-03	1.15E-03	0.48
	U^2			2.04	1.52	1.78	
NH_4^+-N	U_I^2	6.05E-04	0.95	0.07	0.13	0.10	31.49
	U_S^2	6.39E-07	0.01	1.53E-03	1.29E-03	1.39E-03	0.57
	U_P^2	2.28E-03	0.98	0.24	0.25	0.24	58.83
	U_{PI}^2	5.80E-04	0.20	0.01	0.03	0.02	7.42
	U_v^2	2.05E-06	9.71E-03	1.26E-03	4.61E-05	6.64E-04	1.68
	U^2			0.32	0.40	0.36	
NO_3^--N	U_I^2	5.17E-03	4.14	0.33	0.46	0.39	18.04
	U_S^2	1.85E-05	0.92	0.06	0.16	0.11	2.89
	U_P^2	9.94E-03	9.33	1.47	1.91	1.67	63.48
	U_{PI}^2	2.13E-03	1.49	0.10	0.19	0.14	6.24
	U_v^2	1.71E-05	1.59	0.25	0.01	0.13	9.36
	U^2			2.20	2.72	2.45	
TN	U_I^2	5.13E-03	9.62	0.55	1.07	0.80	22.51
	U_S^2	3.48E-05	0.89	0.07	0.15	0.11	1.57
	U_P^2	2.33E-02	15.88	2.75	3.31	3.01	61.64
	U_{PI}^2	6.23E-03	2.65	0.16	0.32	0.24	6.12
	U_v^2	5.24E-05	1.85	0.28	0.01	0.15	8.15
	U^2			3.81	4.86	4.30	

Min/Max: the minimal/maximal value of streamflow or N loading; U_I^2, U_S^2, U_P^2, U_{PI}^2, U_v^2 and U^2: variance of input, structure, parameter, interaction effect, internal variability and total; The gray shadow denotes where values are greater in the rice-growing season than in the fallow season.

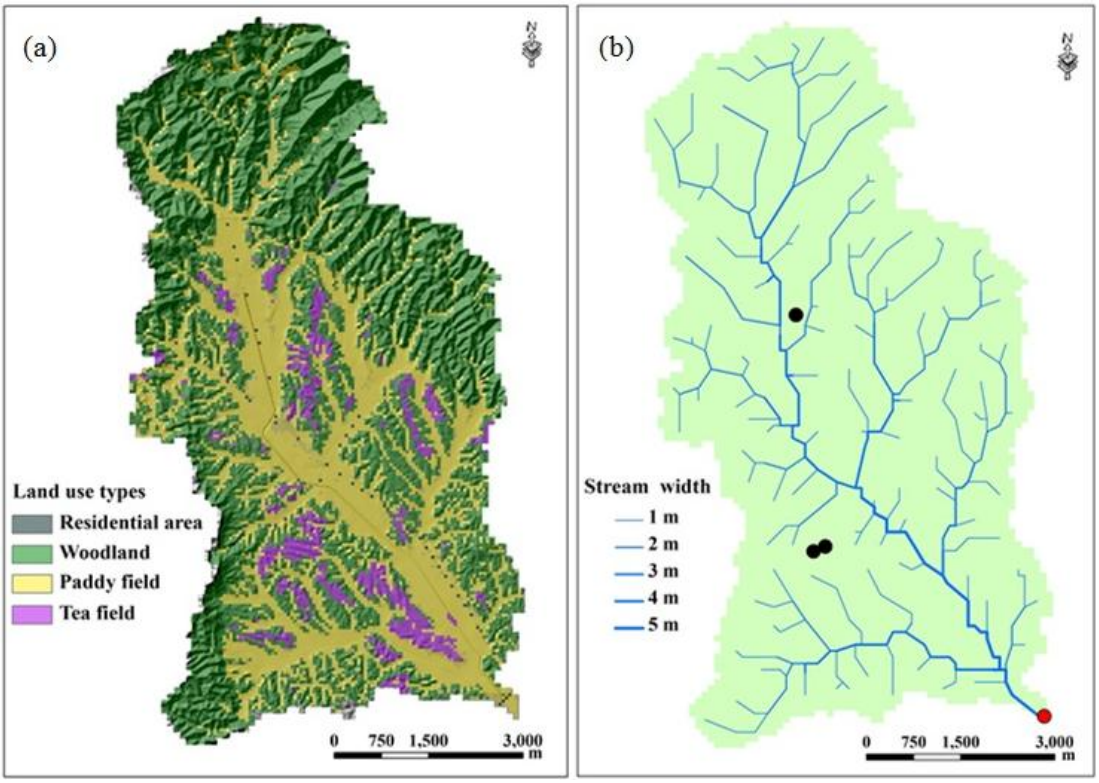

Fig. 1 Land use types (a) and stream network (b) of the Tuojia watershed (The red point is the location of the watershed outlet and stream discharge station. The black points denote locations of meteorological stations).

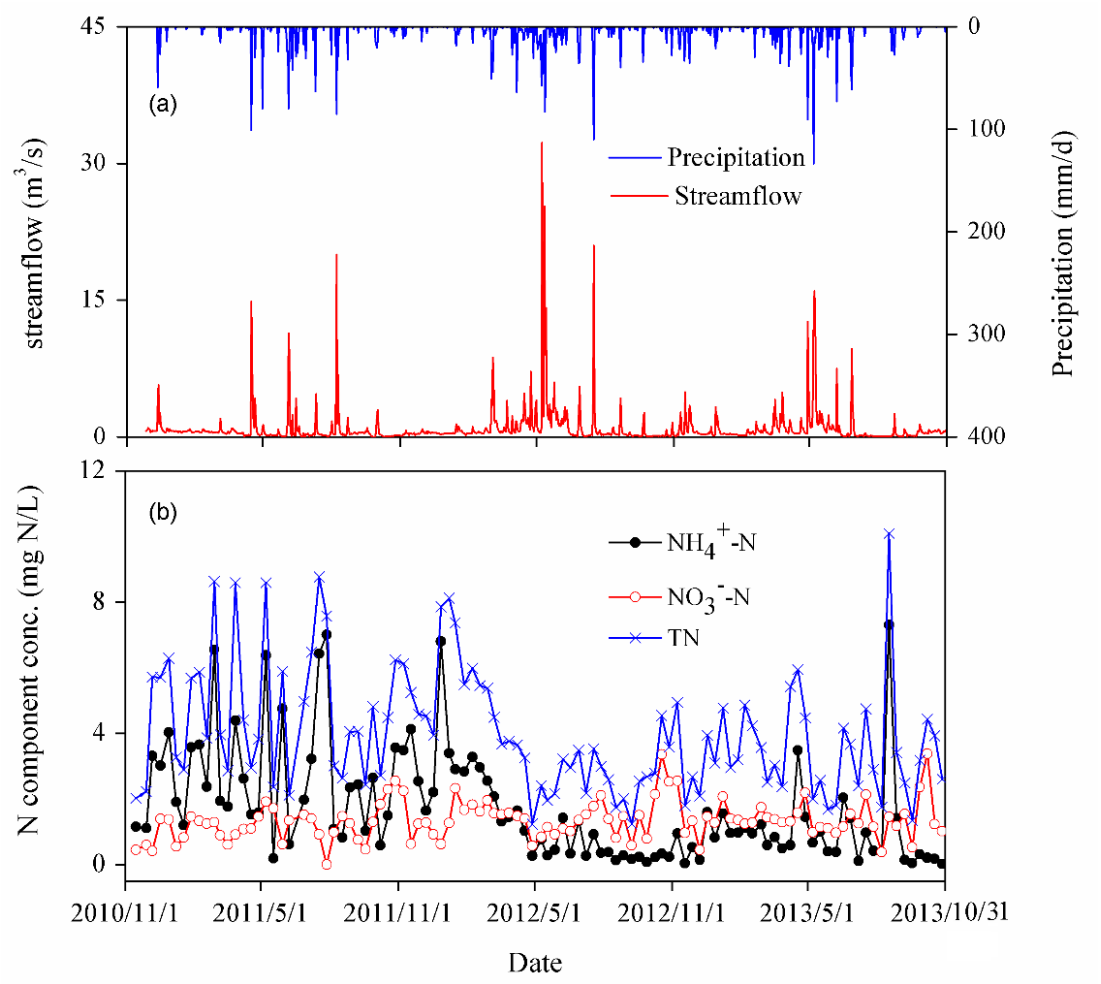

Fig. 2 Measured precipitation, streamflow discharge (a) and N concentrations (b) at outlet of the Tuojia watershed.

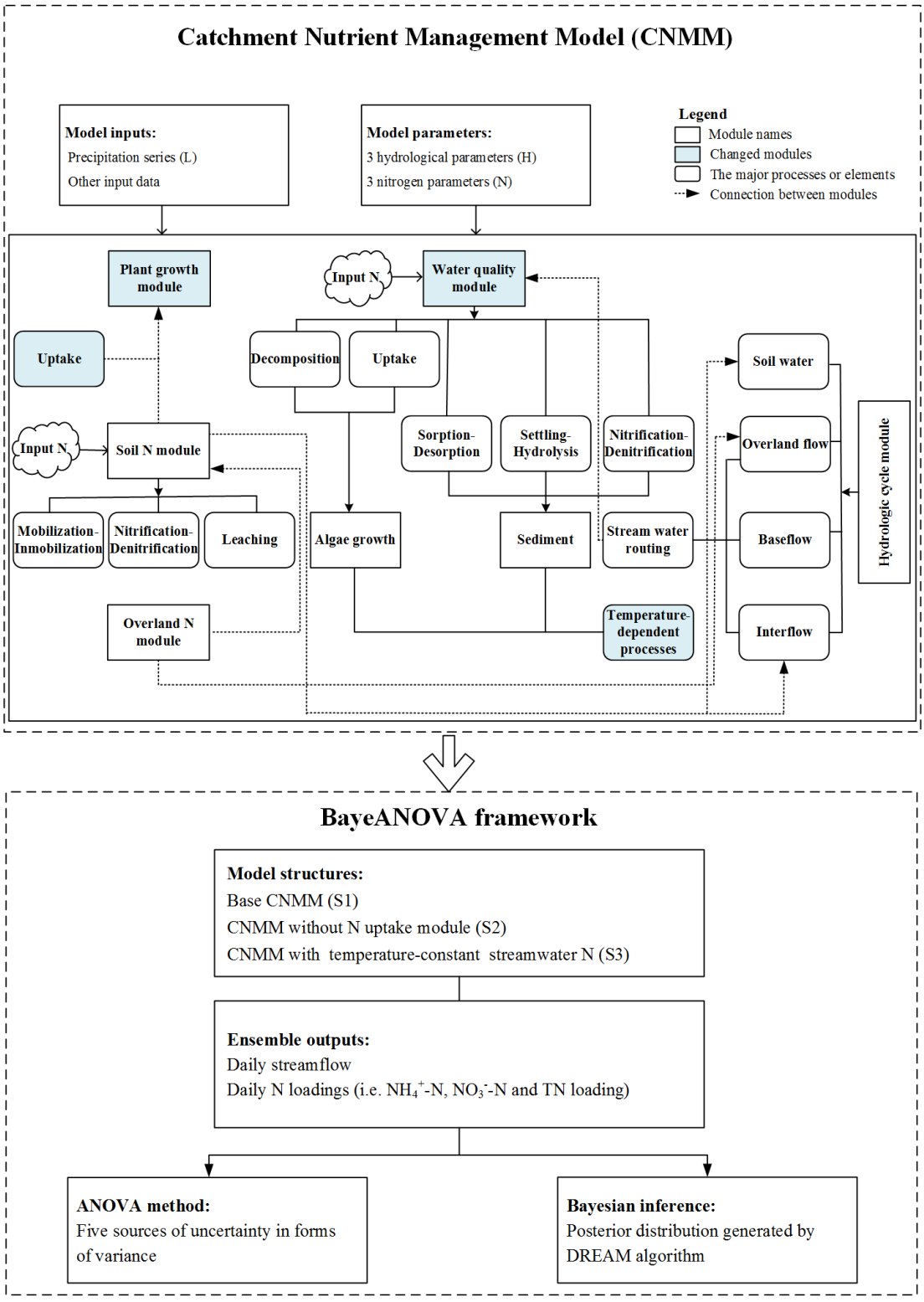

Fig. 3 Flowchart of this study, including the configuration of CNMM and the BayeANOVA framework with DREAM algorithm.

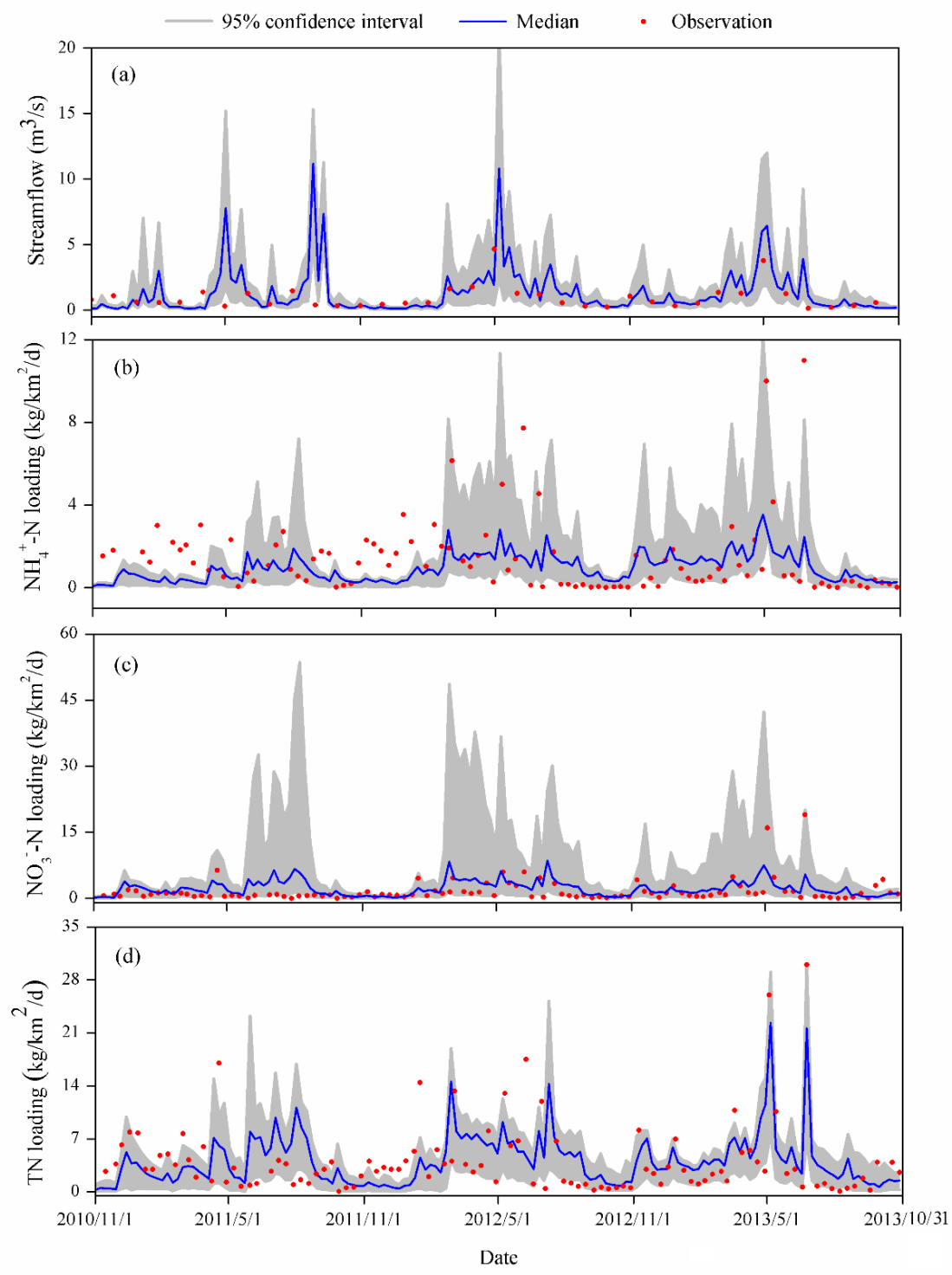

Fig. 4 Estimated 95% predicting confidence intervals of streamflow (a) and NH_4^+-N (b), NO_3^--N (c) and TN (d) loadings during 2010.11-2013.10.

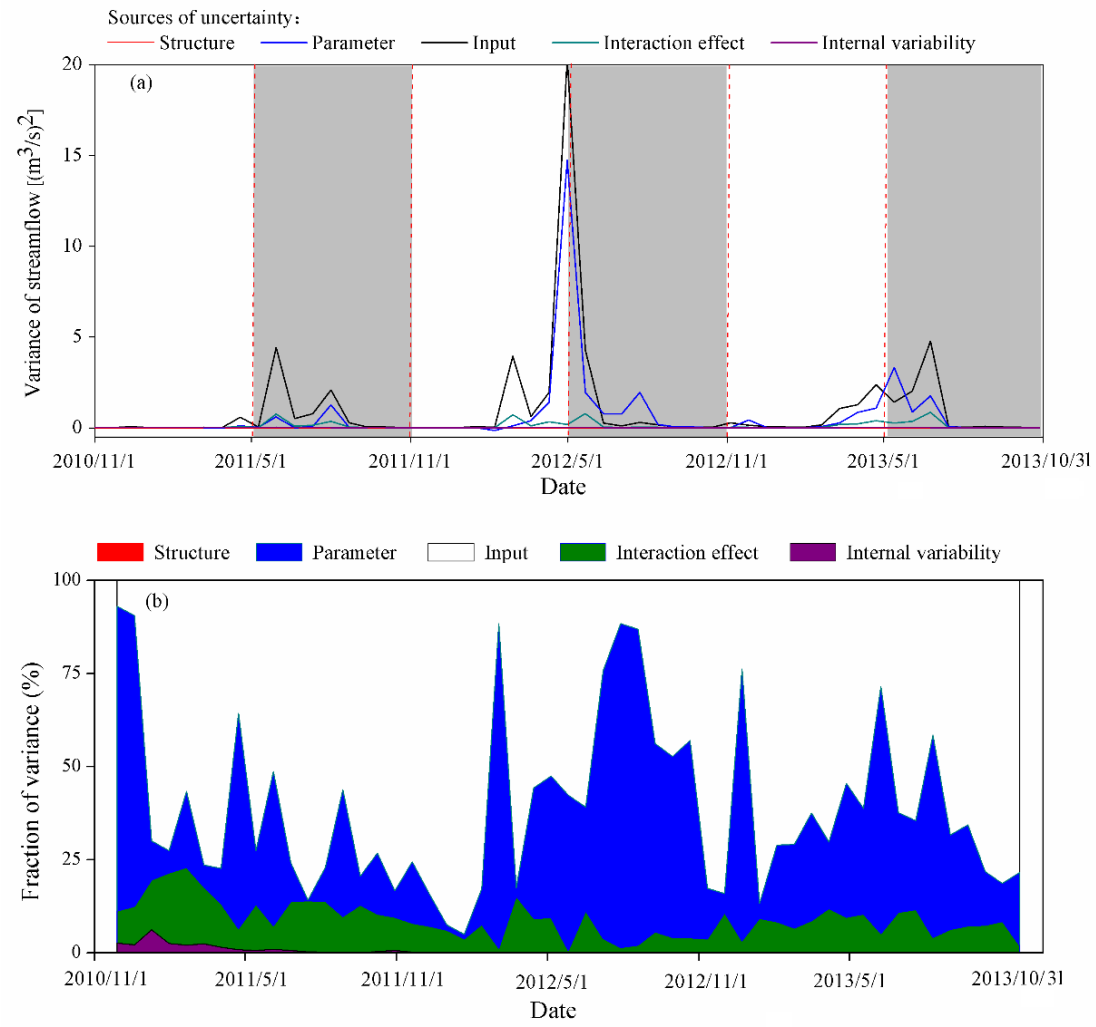

Fig. 5 Variance of simulated streamflow (a) and its fractional variance among five sources (b) during 2010.11-2013.10 in the rice-growing and fallow season. The gray bands indicate the rice-growing season.

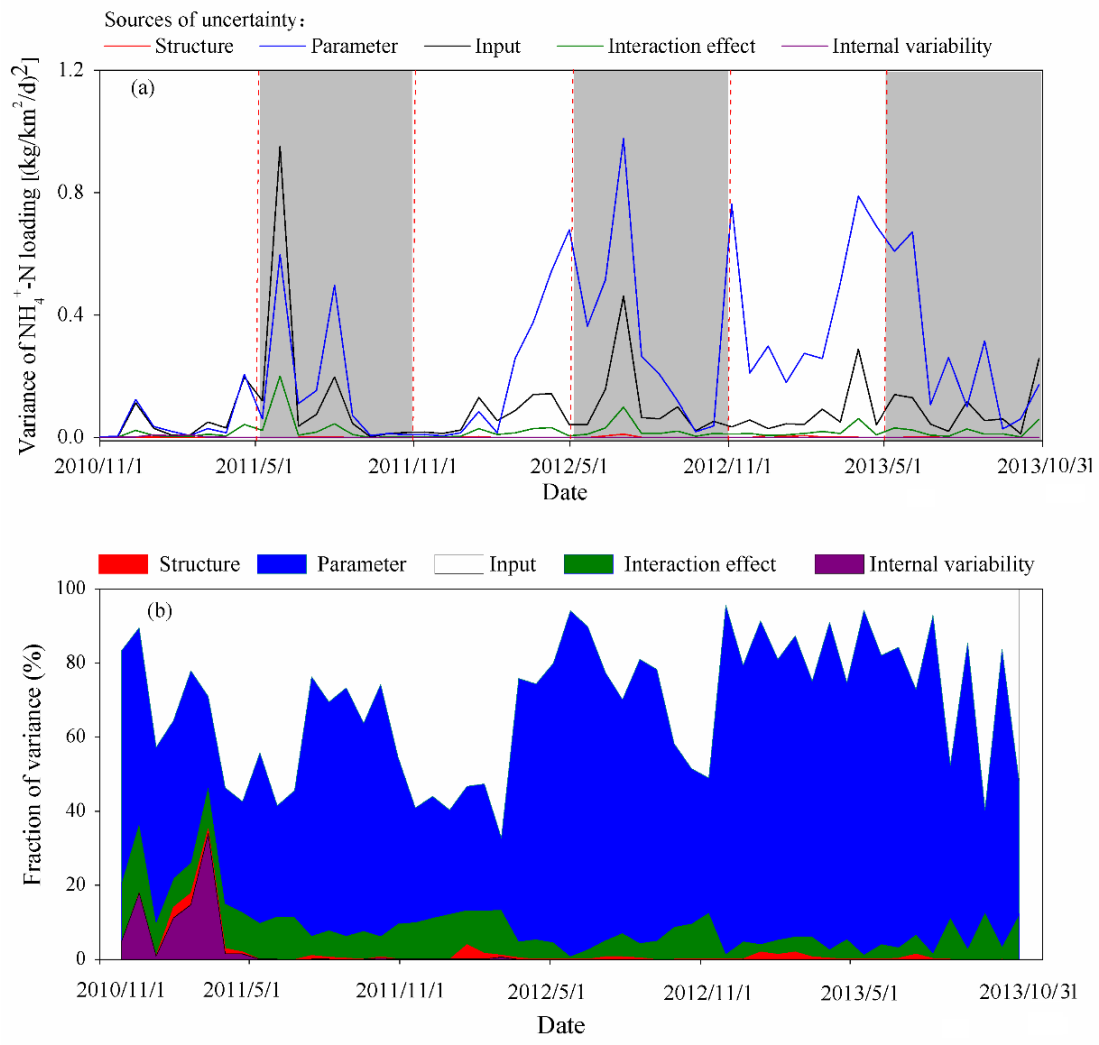

Fig. 6 Variance of simulated NH_4^+-N loading (a) and its fractional variance among five sources (b) during 2010.11-2013.10 in the rice-growing and fallow season. The gray bands indicate the rice-growing season.

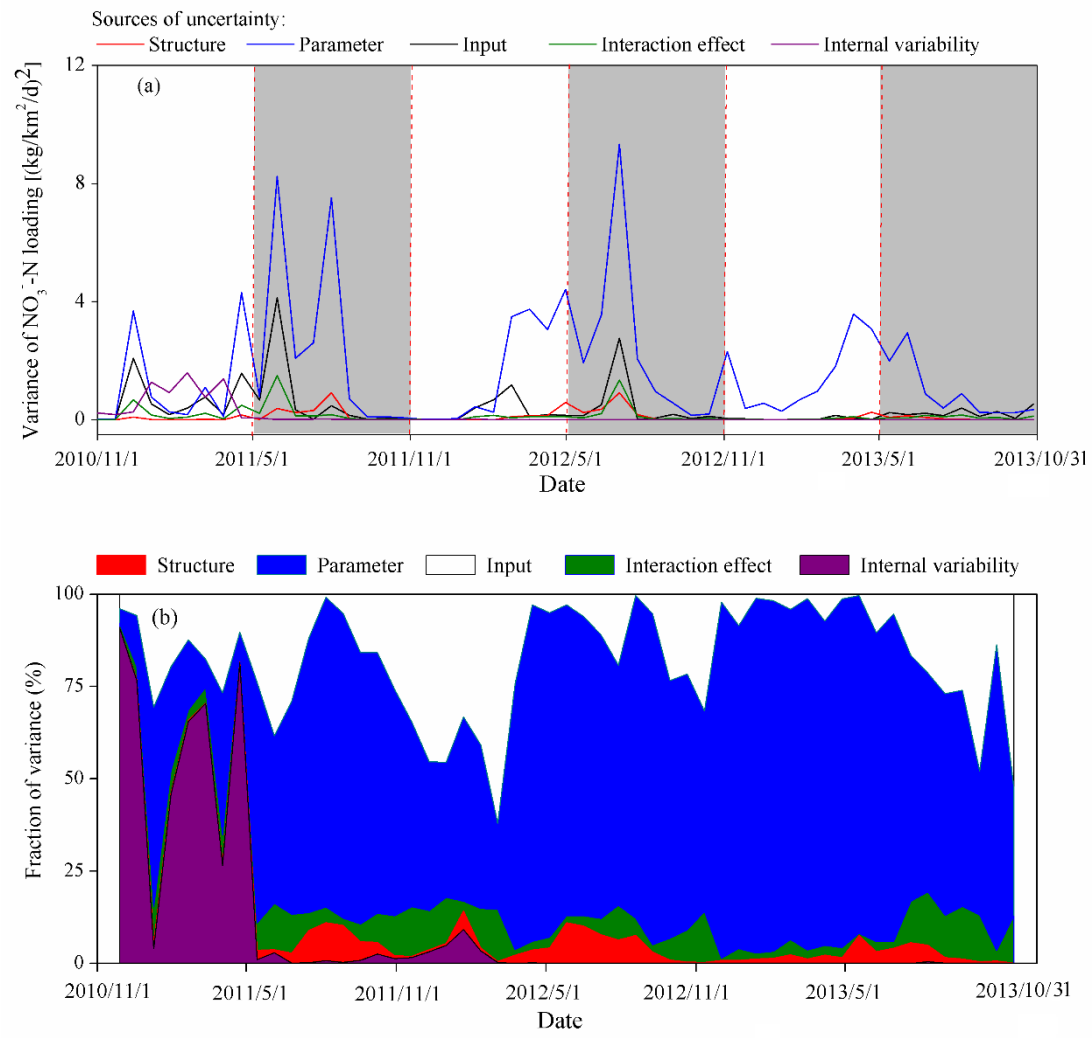

Fig. 7 Variance of simulated NO_3^--N loading (a) and its fractional variance among five sources (b) during 2010.11-2013.10 in the rice-growing and fallow season. The gray bands indicate the rice-growing season.

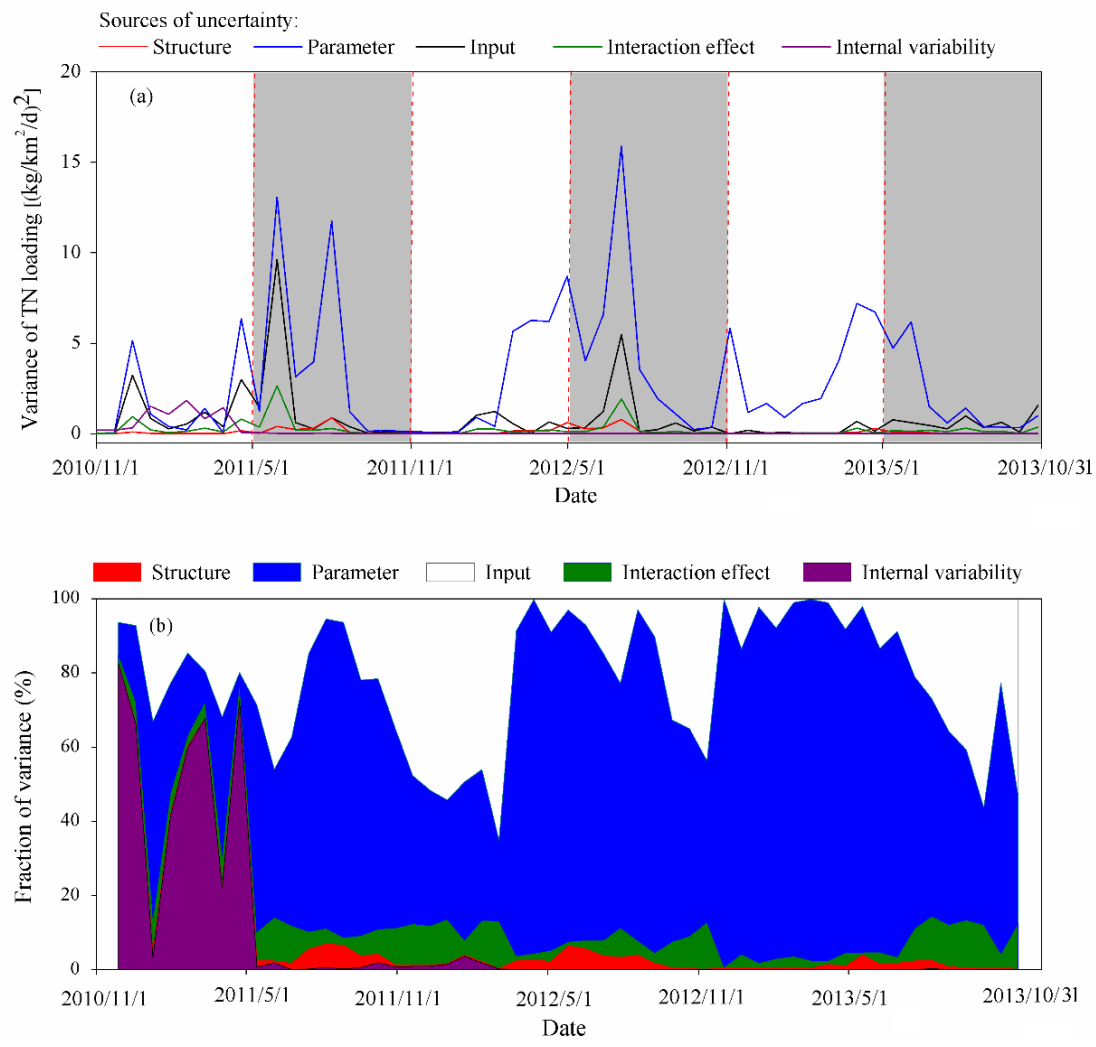

Fig. 8 Variance of simulated TN loading (a) and its fractional variance among five sources (b) during 2010.11-2013.10 in the rice-growing and fallow season. The gray bands indicate the rice-growing season.

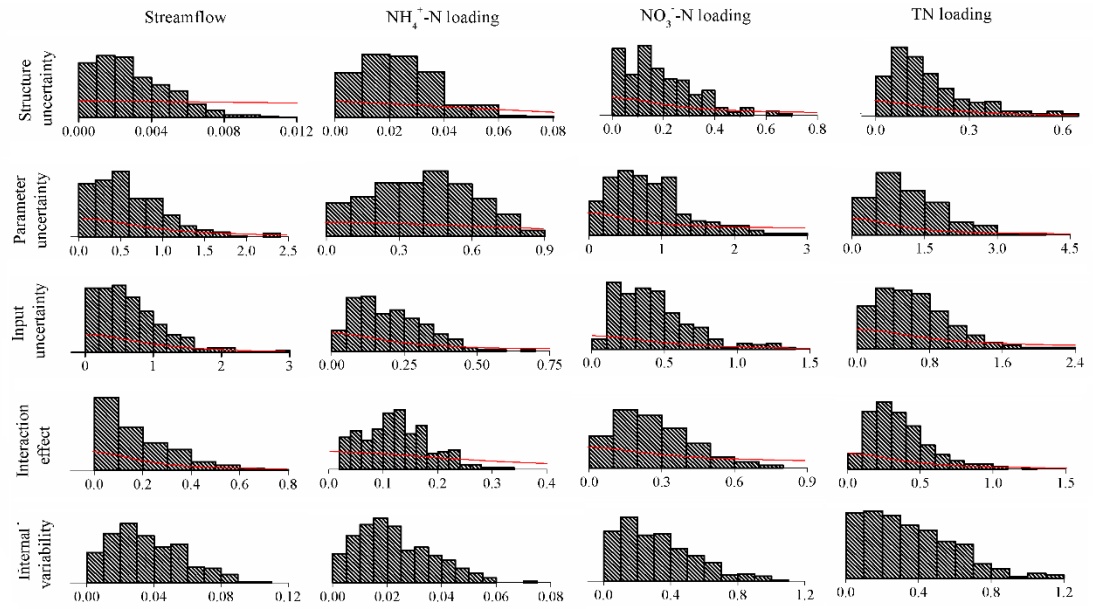

Fig. 9 Posterior distributions (histograms) of superpopulation standard deviations $(\sigma_S, \sigma_P, \sigma_I, \sigma_{PI}, \sigma_v)$ against half-Cauchy prior trends (red lines).

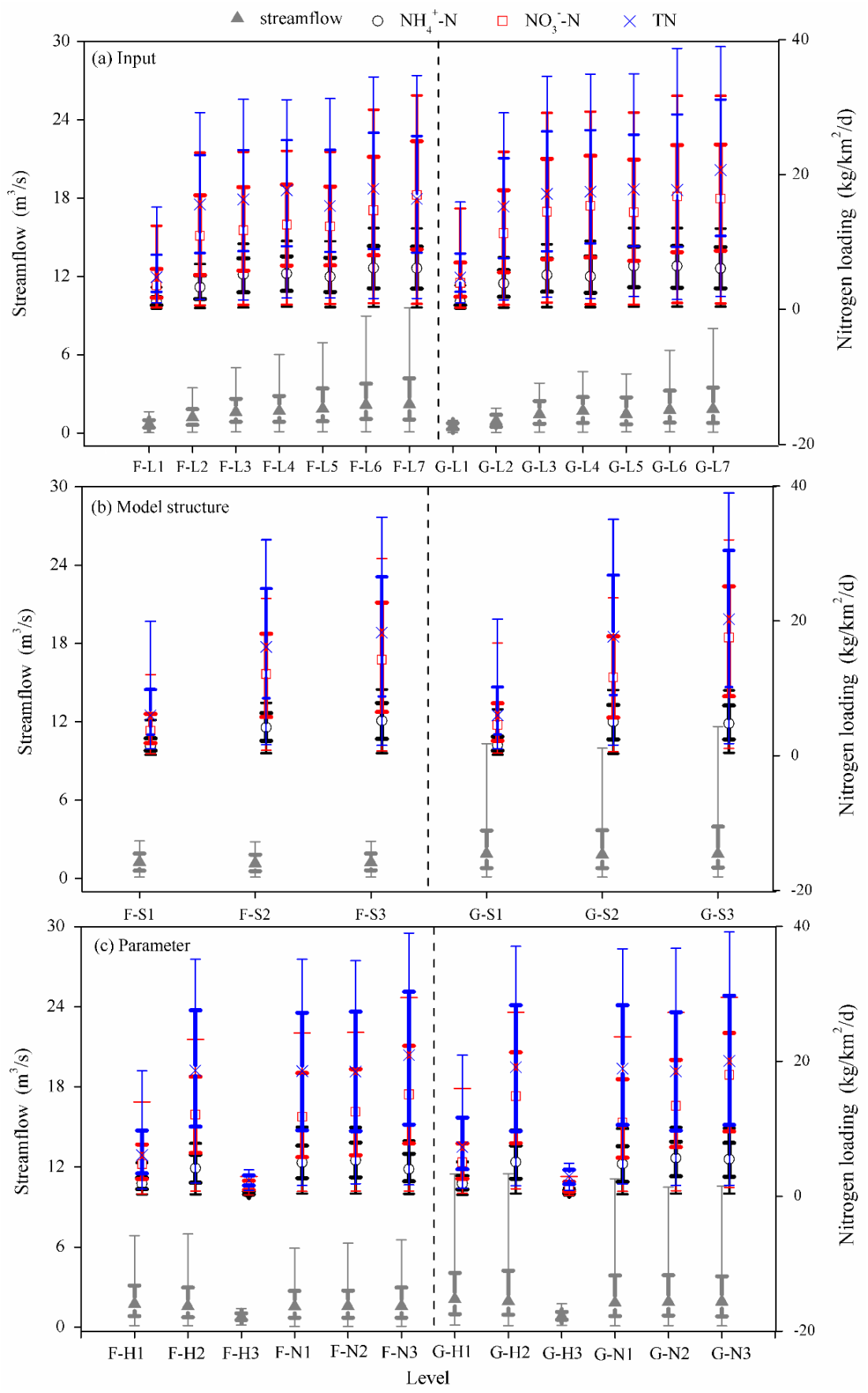

Fig. 10 Statistics of posterior distributions for uncertainty in simulating streamflow and loadings

of NH_4^+-N, NO_3^--N and TN under individual precipitation inputs (a), model structures (b) and parameter sets (c). The thin lines denote the 5th-95th percentiles and the thick lines represent the 25th-75th percentiles.

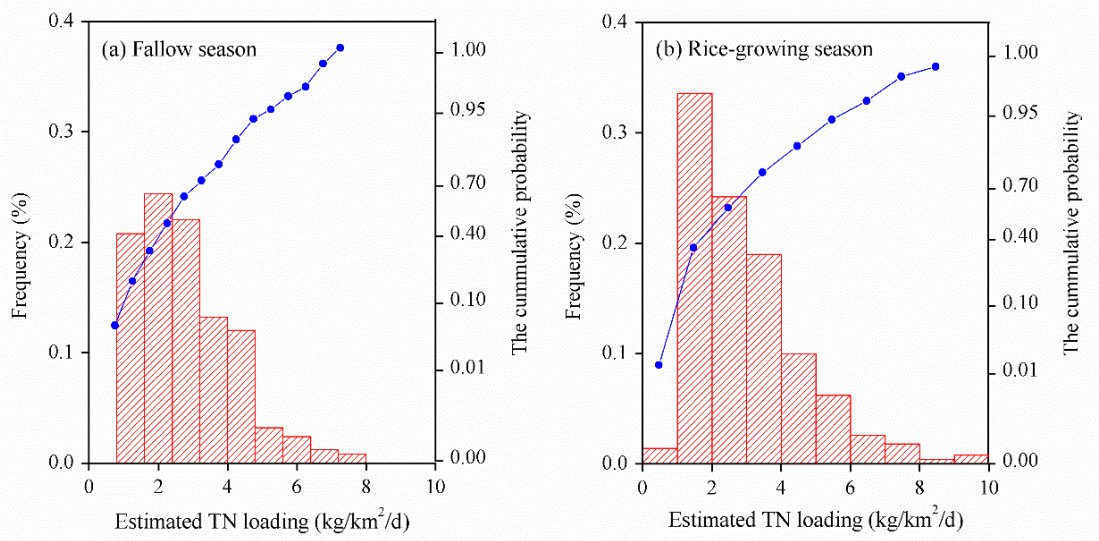

Fig. 11 Estimated values of TN loading and corresponding cumulative probability in the fallow season (a) and rice-growing season (b) during the study period.